Cross section measurement of $e^+e^- \to p\bar{p}\eta$ and $e^+e^- \to p\bar{p}\omega$ at center-of-mass energies between 3.773 GeV and 4.6 GeV

M. Ablikim,[1] M. N. Achasov,[10,c] P. Adlarson,[64] S. Ahmed,[15] M. Albrecht,[4] A. Amoroso,[63a,63c] Q. An,[60,48] Anita,[21] Y. Bai,[47] O. Bakina,[29] R. Baldini Ferroli,[23a] I. Balossino,[24a] Y. Ban,[38,k] K. Begzsuren,[26] J. V. Bennett,[5] N. Berger,[28] M. Bertani,[23a] D. Bettoni,[24a] F. Bianchi,[63a,63c] J. Biernat,[64] J. Bloms,[57] A. Bortone,[63a,63c] I. Boyko,[29] R. A. Briere,[5] H. Cai,[65] X. Cai,[1,48] A. Calcaterra,[23a] G. F. Cao,[1,52] N. Cao,[1,52] S. A. Cetin,[51b] J. F. Chang,[1,48] W. L. Chang,[1,52] G. Chelkov,[29,b] D. Y. Chen,[6] G. Chen,[1] H. S. Chen,[1,52] M. L. Chen,[1,48] S. J. Chen,[36] X. R. Chen,[25] Y. B. Chen,[1,48] Z. J. Chen,[20,l] W. S. Cheng,[63c] G. Cibinetto,[24a] F. Cossio,[63c] X. F. Cui,[37] H. L. Dai,[1,48] J. P. Dai,[42,g] X. C. Dai,[1,52] A. Dbeyssi,[15] R. B. de Boer,[4] D. Dedovich,[29] Z. Y. Deng,[1] A. Denig,[28] I. Denysenko,[29] M. Destefanis,[63a,63c] F. De Mori,[63a,63c] Y. Ding,[34] C. Dong,[37] J. Dong,[1,48] L. Y. Dong,[1,52] M. Y. Dong,[1,48,52] S. X. Du,[68] J. Fang,[1,48] S. S. Fang,[1,52] Y. Fang,[1] R. Farinelli,[24a] L. Fava,[63b,63c] F. Feldbauer,[4] G. Felici,[23a] C. Q. Feng,[60,48] M. Fritsch,[4] C. D. Fu,[1] Y. Fu,[1] X. L. Gao,[60,48] Y. Gao,[61] Y. Gao,[38,k] Y. G. Gao,[6] I. Garzia,[24a,24b] E. M. Gersabeck,[55] A. Gilman,[56] K. Goetzen,[11] L. Gong,[37] W. X. Gong,[1,48] W. Gradl,[28] M. Greco,[63a,63c] L. M. Gu,[36] M. H. Gu,[1,48] S. Gu,[2] Y. T. Gu,[13] C. Y. Guan,[1,52] A. Q. Guo,[22] L. B. Guo,[35] R. P. Guo,[40] Y. P. Guo,[9,h] Y. P. Guo,[28] A. Guskov,[29] S. Han,[65] T. T. Han,[41] T. Z. Han,[9,h] X. Q. Hao,[16] F. A. Harris,[53] K. L. He,[1,52] F. H. Heinsius,[4] T. Held,[4] Y. K. Heng,[1,48,52] M. Himmelreich,[11,f] T. Holtmann,[4] Y. R. Hou,[52] Z. L. Hou,[1] H. M. Hu,[1,52] J. F. Hu,[42,g] T. Hu,[1,48,52] Y. Hu,[1] G. S. Huang,[60,48] L. Q. Huang,[61] X. T. Huang,[41] Y. P. Huang,[1] Z. Huang,[38,k] N. Huesken,[57] T. Hussain,[62] W. Ikegami Andersson,[64] W. Imoehl,[22] M. Irshad,[60,48] S. Jaeger,[4] S. Janchiv,[26,j] Q. Ji,[1] Q. P. Ji,[16] X. B. Ji,[1,52] X. L. Ji,[1,48] H. B. Jiang,[41] X. S. Jiang,[1,48,52] X. Y. Jiang,[37] J. B. Jiao,[41] Z. Jiao,[18] S. Jin,[36] Y. Jin,[54] T. Johansson,[64] N. Kalantar-Nayestanaki,[31] X. S. Kang,[34] R. Kappert,[31] M. Kavatsyuk,[31] B. C. Ke,[43,1] I. K. Keshk,[4] A. Khoukaz,[57] P. Kiese,[28] R. Kiuchi,[1] R. Kliemt,[11] L. Koch,[30] O. B. Kolcu,[51b,e] B. Kopf,[4] M. Kuemmel,[4] M. Kuessner,[4] A. Kupsc,[64] M. G. Kurth,[1,52] W. Kühn,[30] J. J. Lane,[55] J. S. Lange,[30] P. Larin,[15] L. Lavezzi,[63c] H. Leithoff,[28] M. Lellmann,[28] T. Lenz,[28] C. Li,[39] C. H. Li,[33] Cheng Li,[60,48] D. M. Li,[68] F. Li,[1,48] G. Li,[1] H. B. Li,[1,52] H. J. Li,[9,h] J. L. Li,[41] J. Q. Li,[4] Ke Li,[1] L. K. Li,[1] Lei Li,[3] P. L. Li,[60,48] P. R. Li,[32] S. Y. Li,[50] W. D. Li,[1,52] W. G. Li,[1] X. H. Li,[60,48] X. L. Li,[41] Z. B. Li,[49] Z. Y. Li,[49] H. Liang,[60,48] H. Liang,[1,52] Y. F. Liang,[45] Y. T. Liang,[25] L. Z. Liao,[1,52] J. Libby,[21] C. X. Lin,[49] B. Liu,[42,g] B. J. Liu,[1] C. X. Liu,[1] D. Liu,[60,48] D. Y. Liu,[42,g] F. H. Liu,[44] Fang Liu,[1] Feng Liu,[6] H. B. Liu,[13] H. M. Liu,[1,52] Huanhuan Liu,[1] Huihui Liu,[17] J. B. Liu,[60,48] J. Y. Liu,[1,52] K. Liu,[1] K. Y. Liu,[34] Ke Liu,[6] L. Liu,[60,48] Q. Liu,[52] S. B. Liu,[60,48] Shuai Liu,[46] T. Liu,[1,52] X. Liu,[32] Y. B. Liu,[37] Z. A. Liu,[1,48,52] Z. Q. Liu,[41] Y. F. Long,[38,k] X. C. Lou,[1,48,52] F. X. Lu,[16] H. J. Lu,[18] J. D. Lu,[1,52] J. G. Lu,[1,48] X. L. Lu,[1] Y. Lu,[1] Y. P. Lu,[1,48] C. L. Luo,[35] M. X. Luo,[67] P. W. Luo,[49] T. Luo,[9,h] X. L. Luo,[1,48] S. Lusso,[63c] X. R. Lyu,[52] F. C. Ma,[34] H. L. Ma,[1] L. L. Ma,[41] M. M. Ma,[1,52] Q. M. Ma,[1] R. Q. Ma,[1,52] R. T. Ma,[52] X. N. Ma,[37] X. X. Ma,[1,52] X. Y. Ma,[1,48] Y. M. Ma,[41] F. E. Maas,[15] M. Maggiora,[63a,63c] S. Maldaner,[28] S. Malde,[58] Q. A. Malik,[62] A. Mangoni,[23b] Y. J. Mao,[38,k] Z. P. Mao,[1] S. Marcello,[63a,63c] Z. X. Meng,[54] J. G. Messchendorp,[31] G. Mezzadri,[24a] T. J. Min,[36] R. E. Mitchell,[22] X. H. Mo,[1,48,52] Y. J. Mo,[6] N. Yu. Muchnoi,[10,c] H. Muramatsu,[56] S. Nakhoul,[11,f] Y. Nefedov,[29] F. Nerling,[11,f] I. B. Nikolaev,[10,c] Z. Ning,[1,48] S. Nisar,[8,i] S. L. Olsen,[52] Q. Ouyang,[1,48,52] S. Pacetti,[23b,23c] X. Pan,[46] Y. Pan,[55] A. Pathak,[1] P. Patteri,[23a] M. Pelizaeus,[4] H. P. Peng,[60,48] K. Peters,[11,f] J. Pettersson,[64] J. L. Ping,[35] R. G. Ping,[1,52] A. Pitka,[4] R. Poling,[56] V. Prasad,[60,48] H. Qi,[60,48] H. R. Qi,[50] M. Qi,[36] T. Y. Qi,[2] S. Qian,[1,48] W.-B. Qian,[52] Z. Qian,[49] C. F. Qiao,[52] L. Q. Qin,[12] X. P. Qin,[13] X. S. Qin,[4] Z. H. Qin,[1,48] J. F. Qiu,[1] S. Q. Qu,[37] K. H. Rashid,[62] K. Ravindran,[21] C. F. Redmer,[28] A. Rivetti,[63c] V. Rodin,[31] M. Rolo,[63c] G. Rong,[1,52] Ch. Rosner,[15] M. Rump,[57] A. Sarantsev,[29,d] Y. Schelhaas,[28] C. Schnier,[4] K. Schoenning,[64] D. C. Shan,[46] W. Shan,[19] X. Y. Shan,[60,48] M. Shao,[60,48] C. P. Shen,[2] P. X. Shen,[37] X. Y. Shen,[1,52] H. C. Shi,[60,48] R. S. Shi,[1,52] X. Shi,[1,48] X. D. Shi,[60,48] J. J. Song,[41] Q. Q. Song,[60,48] W. M. Song,[27] Y. X. Song,[38,k] S. Sosio,[63a,63c] S. Spataro,[63a,63c] F. F. Sui,[41] G. X. Sun,[1] J. F. Sun,[16] L. Sun,[65] S. S. Sun,[1,52] T. Sun,[1,52] W. Y. Sun,[35] X. Sun,[20,l] Y. J. Sun,[60,48] Y. K. Sun,[60,48] Y. Z. Sun,[1] Z. T. Sun,[1] Y. H. Tan,[65] Y. X. Tan,[60,48] C. J. Tang,[45] G. Y. Tang,[1] J. Tang,[49] V. Thoren,[64] B. Tsednee,[26] I. Uman,[51d] B. Wang,[1] B. L. Wang,[52] C. W. Wang,[36] D. Y. Wang,[38,k] H. P. Wang,[1,52] K. Wang,[1,48] L. L. Wang,[1] M. Wang,[41] M. Z. Wang,[38,k] Meng Wang,[1,52] W. H. Wang,[65] W. P. Wang,[60,48] X. Wang,[38,k] X. F. Wang,[32] X. L. Wang,[9,h] Y. Wang,[60,48] Y. Wang,[49] Y. D. Wang,[15] Y. F. Wang,[1,48,52] Y. Q. Wang,[1] Z. Wang,[1,48] Z. Y. Wang,[1] Ziyi Wang,[52] Zongyuan Wang,[1,52] D. H. Wei,[12] P. Weidenkaff,[28] F. Weidner,[57] S. P. Wen,[1] D. J. White,[55] U. Wiedner,[4] G. Wilkinson,[58] M. Wolke,[64] L. Wollenberg,[4] J. F. Wu,[1,52] L. H. Wu,[1] L. J. Wu,[1,52] X. Wu,[9,h] Z. Wu,[1,48] L. Xia,[60,48] H. Xiao,[9,h] S. Y. Xiao,[1] Y. J. Xiao,[1,52] Z. J. Xiao,[35] X. H. Xie,[38,k] Y. G. Xie,[1,48] Y. H. Xie,[6] T. Y. Xing,[1,52] X. A. Xiong,[1,52] G. F. Xu,[1] J. J. Xu,[36] Q. J. Xu,[14] W. Xu,[1,52] X. P. Xu,[46] L. Yan,[63a,63c] L. Yan,[9,h] W. B. Yan,[60,48] W. C. Yan,[68] Xu Yan,[46] H. J. Yang,[42,g] H. X. Yang,[1] L. Yang,[65] R. X. Yang,[60,48] S. L. Yang,[1,52] Y. H. Yang,[36] Y. X. Yang,[12] Yifan Yang,[1,52] Zhi Yang,[25] M. Ye,[1,48] M. H. Ye,[7] J. H. Yin,[1] Z. Y. You,[49] B. X. Yu,[1,48,52] C. X. Yu,[37] G. Yu,[1,52] J. S. Yu,[20,l] T. Yu,[61] C. Z. Yuan,[1,52] W. Yuan,[63a,63c] X. Q. Yuan,[38,k] Y. Yuan,[1] Z. Y. Yuan,[49] C. X. Yue,[33] A. Yuncu,[51b,a] A. A. Zafar,[62] Y. Zeng,[20,l] B. X. Zhang,[1] Guangyi Zhang,[16] H. H. Zhang,[49] H. Y. Zhang,[1,48] J. L. Zhang,[66] J. Q. Zhang,[4] J. W. Zhang,[1,48,52] J. Y. Zhang,[1] J. Z. Zhang,[1,52] Jianyu Zhang,[1,52]

Jiawei Zhang,[1,52] L. Zhang,[1] Lei Zhang,[36] S. Zhang,[49] S. F. Zhang,[36] T. J. Zhang,[42,g] X. Y. Zhang,[41] Y. Zhang,[58] Y. H. Zhang,[1,48] Y. T. Zhang,[60,48] Yan Zhang,[60,48] Yao Zhang,[1] Yi Zhang,[9,h] Z. H. Zhang,[6] Z. Y. Zhang,[65] G. Zhao,[1] J. Zhao,[33] J. Y. Zhao,[1,52] J. Z. Zhao,[1,48] Lei Zhao,[60,48] Ling Zhao,[1] M. G. Zhao,[37] Q. Zhao,[1] S. J. Zhao,[68] Y. B. Zhao,[1,48] Y. X. Zhao,[25] Z. G. Zhao,[60,48] A. Zhemchugov,[29,b] B. Zheng,[61] J. P. Zheng,[1,48] Y. Zheng,[38,k] Y. H. Zheng,[52] B. Zhong,[35] C. Zhong,[61] L. P. Zhou,[1,52] Q. Zhou,[1,52] X. Zhou,[65] X. K. Zhou,[52] X. R. Zhou,[60,48] A. N. Zhu,[1,52] J. Zhu,[37] K. Zhu,[1] K. J. Zhu,[1,48,52] S. H. Zhu,[59] W. J. Zhu,[37] X. L. Zhu,[50] Y. C. Zhu,[60,48] Z. A. Zhu,[1,52] B. S. Zou,[1] and J. H. Zou[1]

(BESIII Collaboration)

[1]*Institute of High Energy Physics, Beijing 100049, People's Republic of China*
[2]*Beihang University, Beijing 100191, People's Republic of China*
[3]*Beijing Institute of Petrochemical Technology, Beijing 102617, People's Republic of China*
[4]*Bochum Ruhr-University, D-44780 Bochum, Germany*
[5]*Carnegie Mellon University, Pittsburgh, Pennsylvania 15213, USA*
[6]*Central China Normal University, Wuhan 430079, People's Republic of China*
[7]*China Center of Advanced Science and Technology, Beijing 100190, People's Republic of China*
[8]*COMSATS University Islamabad, Lahore Campus, Defence Road, Off Raiwind Road, 54000 Lahore, Pakistan*
[9]*Fudan University, Shanghai 200443, People's Republic of China*
[10]*G.I. Budker Institute of Nuclear Physics SB RAS (BINP), Novosibirsk 630090, Russia*
[11]*GSI Helmholtzcentre for Heavy Ion Research GmbH, D-64291 Darmstadt, Germany*
[12]*Guangxi Normal University, Guilin 541004, People's Republic of China*
[13]*Guangxi University, Nanning 530004, People's Republic of China*
[14]*Hangzhou Normal University, Hangzhou 310036, People's Republic of China*
[15]*Helmholtz Institute Mainz, Johann-Joachim-Becher-Weg 45, D-55099 Mainz, Germany*
[16]*Henan Normal University, Xinxiang 453007, People's Republic of China*
[17]*Henan University of Science and Technology, Luoyang 471003, People's Republic of China*
[18]*Huangshan College, Huangshan 245000, People's Republic of China*
[19]*Hunan Normal University, Changsha 410081, People's Republic of China*
[20]*Hunan University, Changsha 410082, People's Republic of China*
[21]*Indian Institute of Technology Madras, Chennai 600036, India*
[22]*Indiana University, Bloomington, Indiana 47405, USA*
[23a]*INFN Laboratori Nazionali di Frascati, I-00044 Frascati, Italy*
[23b]*INFN Sezione di Perugia, I-06100 Perugia, Italy*
[23c]*University of Perugia, I-06100 Perugia, Italy*
[24a]*INFN Sezione di Ferrara, I-44122 Ferrara, Italy*
[24b]*University of Ferrara, I-44122 Ferrara, Italy*
[25]*Institute of Modern Physics, Lanzhou 730000, People's Republic of China*
[26]*Institute of Physics and Technology, Peace Avenue 54B, Ulaanbaatar 13330, Mongolia*
[27]*Jilin University, Changchun 130012, People's Republic of China*
[28]*Johannes Gutenberg University of Mainz, Johann-Joachim-Becher-Weg 45, D-55099 Mainz, Germany*
[29]*Joint Institute for Nuclear Research, 141980 Dubna, Moscow region, Russia*
[30]*Justus-Liebig-Universitaet Giessen, II. Physikalisches Institut, Heinrich-Buff-Ring 16, D-35392 Giessen, Germany*
[31]*KVI-CART, University of Groningen, NL-9747 AA Groningen, Netherlands*
[32]*Lanzhou University, Lanzhou 730000, People's Republic of China*
[33]*Liaoning Normal University, Dalian 116029, People's Republic of China*
[34]*Liaoning University, Shenyang 110036, People's Republic of China*
[35]*Nanjing Normal University, Nanjing 210023, People's Republic of China*
[36]*Nanjing University, Nanjing 210093, People's Republic of China*
[37]*Nankai University, Tianjin 300071, People's Republic of China*
[38]*Peking University, Beijing 100871, People's Republic of China*
[39]*Qufu Normal University, Qufu 273165, People's Republic of China*
[40]*Shandong Normal University, Jinan 250014, People's Republic of China*
[41]*Shandong University, Jinan 250100, People's Republic of China*
[42]*Shanghai Jiao Tong University, Shanghai 200240, People's Republic of China*
[43]*Shanxi Normal University, Linfen 041004, People's Republic of China*
[44]*Shanxi University, Taiyuan 030006, People's Republic of China*
[45]*Sichuan University, Chengdu 610064, People's Republic of China*
[46]*Soochow University, Suzhou 215006, People's Republic of China*

[47]*Southeast University, Nanjing 211100, People's Republic of China*
[48]*State Key Laboratory of Particle Detection and Electronics, Beijing 100049, Hefei 230026, People's Republic of China*
[49]*Sun Yat-Sen University, Guangzhou 510275, People's Republic of China*
[50]*Tsinghua University, Beijing 100084, People's Republic of China*
[51a]*Ankara University, 06100 Tandogan, Ankara, Turkey*
[51b]*Istanbul Bilgi University, 34060 Eyup, Istanbul, Turkey*
[51c]*Uludag University, 16059 Bursa, Turkey*
[51d]*Near East University, Nicosia, North Cyprus, Mersin 10, Turkey*
[52]*University of Chinese Academy of Sciences, Beijing 100049, People's Republic of China*
[53]*University of Hawaii, Honolulu, Hawaii 96822, USA*
[54]*University of Jinan, Jinan 250022, People's Republic of China*
[55]*University of Manchester, Oxford Road, Manchester M13 9PL, United Kingdom*
[56]*University of Minnesota, Minneapolis, Minnesota 55455, USA*
[57]*University of Muenster, Wilhelm-Klemm-Straße 9, 48149 Muenster, Germany*
[58]*University of Oxford, Keble Rd, Oxford, United Kingdom OX13RH*
[59]*University of Science and Technology Liaoning, Anshan 114051, People's Republic of China*
[60]*University of Science and Technology of China, Hefei 230026, People's Republic of China*
[61]*University of South China, Hengyang 421001, People's Republic of China*
[62]*University of the Punjab, Lahore-54590, Pakistan*
[63a]*University of Turin, I-10125 Turin, Italy*
[63b]*University of Eastern Piedmont, I-15121 Alessandria, Italy*
[63c]*INFN, I-10125 Turin, Italy*
[64]*Uppsala University, Box 516, SE-75120 Uppsala, Sweden*
[65]*Wuhan University, Wuhan 430072, People's Republic of China*
[66]*Xinyang Normal University, Xinyang 464000, People's Republic of China*
[67]*Zhejiang University, Hangzhou 310027, People's Republic of China*
[68]*Zhengzhou University, Zhengzhou 450001, People's Republic of China*

(Received 9 February 2021; accepted 7 October 2021; published 22 November 2021)

Based on 14.7 fb^{-1} of e^+e^- annihilation data collected with the BESIII detector at the BEPCII collider at 17 different center-of-mass energies between 3.7730 GeV and 4.5995 GeV, Born cross sections of the two processes $e^+e^- \to p\bar{p}\eta$ and $e^+e^- \to p\bar{p}\omega$ are measured for the first time. No indication of resonant production through a vector state V is observed, and upper limits on the Born cross sections of $e^+e^- \to V \to p\bar{p}\eta$ and $e^+e^- \to V \to p\bar{p}\omega$ at the 90% confidence level are calculated for a large parameter space in resonance masses and widths. For the current world average parameters of the $\psi(4230)$ of $m = 4.2187$ GeV/c^2 and $\Gamma = 44$ MeV, we find upper limits on resonant production of the $p\bar{p}\eta$ and $p\bar{p}\omega$ final states of 7.5 pb and 10.4 pb at the 90% CL, respectively.

DOI: 10.1103/PhysRevD.104.092008

[a]Also at Bogazici University, 34342 Istanbul, Turkey.
[b]Also at the Moscow Institute of Physics and Technology, Moscow 141700, Russia.
[c]Also at the Novosibirsk State University, Novosibirsk 630090, Russia.
[d]Also at the NRC "Kurchatov Institute," PNPI, 188300 Gatchina, Russia.
[e]Also at Istanbul Arel University, 34295 Istanbul, Turkey.
[f]Also at Goethe University Frankfurt, 60323 Frankfurt am Main, Germany.
[g]Also at Key Laboratory for Particle Physics, Astrophysics and Cosmology, Ministry of Education; Shanghai Key Laboratory for Particle Physics and Cosmology; Institute of Nuclear and Particle Physics, Shanghai 200240, People's Republic of China.
[h]Also at Key Laboratory of Nuclear Physics and Ion-beam Application (MOE) and Institute of Modern Physics, Fudan University, Shanghai 200443, People's Republic of China.
[i]Also at Harvard University, Department of Physics, Cambridge, Massachusetts 02138, USA.
[j]Currently at: Institute of Physics and Technology, Peace Avenue 54B, Ulaanbaatar 13330, Mongolia.
[k]Also at State Key Laboratory of Nuclear Physics and Technology, Peking University, Beijing 100871, People's Republic of China.
[l]School of Physics and Electronics, Hunan University, Changsha 410082, China.

I. INTRODUCTION

In recent years, several unexpected states have been discovered in the charmonium sector. Notable examples are the $\chi_{c1}(3872)$ discovered by Belle [1], the charged charmoniumlike $Z_c(3900)$ discovered by BESIII [2] and the vector states $\psi(4220)$ and $\psi(4390)$, originally discovered by *BABAR* [3] as a single broad resonance named $Y(4260)$ in the $e^+e^- \to \gamma_{\rm ISR}\pi^+\pi^- J/\psi$ process, and later found to be two distinct states by BESIII [4]. Charmoniumlike vector states similar to the $\psi(4220)$ and $\psi(4390)$ were observed by BESIII in the processes $e^+e^- \to \pi^+\pi^- h_c$ [5], $\pi^+\pi^-\psi(3686)$ [6], $D^0D^{*-}\pi^+$ [7], $\omega\chi_{c0}$ [8] and $\eta J/\psi$ [9–11]. However, so far no observations have been made of decays into light mesons or baryons for either the $\psi(4220)$ or the $\psi(4390)$. Cross sections have been determined for the processes $e^+e^- \to p\bar{p}\pi^0$ [12], $\phi\phi\phi$, $\phi\phi\omega$ [13], $pK_S^0\bar{n}K^-$ [14], $K_S^0K^\pm\pi^\mp$ [15], $K_S^0K^\pm\pi^\mp\pi^0$ and $K_S^0K^\pm\pi^\mp\eta$ [16] without significant detection of resonant production. Channels that include a proton antiproton pair are especially interesting, since the partial width of decays of the type $V \to p\bar{p}h$, where V is a vector-state in the charmonium region and h is a light meson, can be related to the production cross section $p\bar{p} \to Vh$ [17]. In light of the upcoming PANDA experiment at the FAIR facility [18], it is important to obtain the production cross sections of potentially exotic resonances in the charmonium sector.

Multiple theoretical explanations have been offered concerning the nature of the $\psi(4220)$ and $\psi(4390)$ states. Possible interpretations include $D_1\bar{D}$ molecules, hybrid charmonia or baryonium states, and their compatibility with experimental data have recently been discussed in detail in Ref. [19]. Additional information is needed from experiments in order to discriminate between the different hypotheses. Thus, the search for new decay modes of the $\psi(4220)$ and $\psi(4390)$ is important.

In this work, we report measurements of the Born cross sections of the processes $e^+e^- \to p\bar{p}\eta$ and $e^+e^- \to p\bar{p}\omega$ for data collected at 17 different center-of-mass (c.m.) energies between $\sqrt{s} = 3.7730$ GeV and 4.5995 GeV with the BESIII detector. The center-of-mass energy dependence of both cross sections is investigated for possible resonant contributions $V \to p\bar{p}\eta$ and $V \to p\bar{p}\omega$.

II. BESIII DETECTOR AND MONTE CARLO SIMULATIONS

The BESIII detector is a magnetic spectrometer [20] located at the Beijing Electron Positron Collider (BEPCII) [21]. The cylindrical core of the BESIII detector consists of a helium-based multilayer drift chamber (MDC), a plastic scintillator time-of-flight system (TOF), and a CsI(Tl) electromagnetic calorimeter (EMC), which are all enclosed in a superconducting solenoidal magnet providing a 1.0 T magnetic field. The solenoid is supported by an octagonal flux-return yoke with resistive plate counter muon identifier modules interleaved with steel. The acceptance of charged particles and photons is 93% over the 4π solid angle. The charged-particle momentum resolution at 1 GeV/c is 0.5%, and the dE/dx resolution is 6% for the electrons from Bhabha scattering. The EMC measures photon energies with a resolution of 2.5% (5%) at 1 GeV in the barrel (end cap) region. The time resolution of the TOF barrel part is 68 ps, while that of the end cap part is 110 ps. The end cap TOF system was upgraded in 2015 with multigap resistive plate chamber technology, providing a time resolution of 60 ps [22]. This improvement affects data at 11 of the 17 center-of-mass energy points.

A Monte Carlo (MC) simulation of the full BESIII detector, based on GEANT4 [23], is used to optimize selection requirements, determine the product of detector acceptance and reconstruction efficiency and study and estimate possible background contributions. These simulations also account for the observed beam energy spread.

Dedicated simulations with 10^6 events per center-of-mass energy of the signal processes $e^+e^- \to p\bar{p}\eta$ and $e^+e^- \to p\bar{p}\omega$ with subsequent decays $\eta \to \gamma\gamma$, $\eta \to \pi^+\pi^-\pi^0$, $\omega \to \pi^+\pi^-\pi^0$, and $\pi^0 \to \gamma\gamma$ are generated with the ConExc [24] generator, accounting for initial state radiation (ISR) and vacuum polarization (VP). The two different decay modes of the η meson are weighted according to their respective branching fraction as given by the Particle Data Group (PDG) Ref. [25].

In addition, an inclusive MC sample at a center-of-mass energy of $\sqrt{s} = 4.1784$ GeV, corresponding to the dataset with the largest integrated luminosity of $L = 3189$ pb^{-1} (see Table I), is used to study potential background contributions. This sample includes open charm processes, ISR production of vector charmonium(like) states and continuum $q\bar{q}$ (where q is a u, d, s quark) processes. Known decay modes are modeled with EVTGEN [26] using branching fractions taken from the PDG [25], whereas unknown processes are modeled by the LUNDCHARM model [27]. Final state radiation (FSR) from charged final state particles is incorporated with the PHOTOS package [28]. The inclusive MC sample at $\sqrt{s} = 4.1784$ GeV corresponds to 40 times the luminosity for the data at this center-of-mass energy.

III. EVENT SELECTION

Two different final states are studied in this work, namely $p\bar{p}\gamma\gamma$ (for $e^+e^- \to p\bar{p}\eta$ with $\eta \to \gamma\gamma$) and $p\bar{p}\pi^+\pi^-\gamma\gamma$ (for $e^+e^- \to p\bar{p}\eta$ with $\eta \to \pi^+\pi^-\pi^0$ and $e^+e^- \to p\bar{p}\omega$ with $\omega \to \pi^+\pi^-\pi^0$, both with a subsequent $\pi^0 \to \gamma\gamma$ decay). In the analysis, the invariant mass distributions $m(\gamma\gamma)$ and $m(\pi^+\pi^-\pi^0)$ will be used to identify and quantify η and ω contributions. The polar angle θ of each charged track detected in the MDC has to satisfy $|\cos\theta| < 0.93$, and its point of closest approach to the interaction point must be within ± 10 cm in the beam direction and within 1 cm in the

TABLE I. Summary of the Born cross sections σ_B of the process $e^+e^- \to p\bar{p}\eta$ for the datasets at different center-of-mass energies $\sqrt{s}$, integrated luminosity L, radiative corrections $1+\delta_r$, vacuum polarization correction $\frac{1}{|1-\Pi|^2}$, number of observed events N_i, efficiency ϵ_i, and cross section σ_i for the two different decays (1) $\eta \to \gamma\gamma$ and (2) $\eta \to \pi^+\pi^-\pi^0$.

$\sqrt{s}$ (GeV)	L (pb^{-1})	$(1+\delta_r)$	$\frac{1}{\lvert 1-\Pi\rvert^2}$	N_1	ε_1 (%)	σ_1 (pb)	N_2	ε_2 (%)	σ_2 (pb)	σ_B (pb)
3.7730	2931.8	0.8993	1.057	$1521.9^{+39.8}_{-38.2}$	36.3 ± 0.1	$3.82^{+0.10}_{-0.10}$	$627.1^{+28.8}_{-27.0}$	24.8 ± 0.1	$4.00^{+0.18}_{-0.17}$	$4.09^{+0.09}_{-0.08} \pm 0.15$
3.8695	224.0	0.9290	1.051	$106.8^{+11.1}_{-9.5}$	34.0 ± 0.1	$3.65^{+0.38}_{-0.32}$	$39.9^{+7.8}_{-6.1}$	22.8 ± 0.1	$3.53^{+0.69}_{-0.54}$	$3.62^{+0.33}_{-0.28} \pm 0.15$
4.0076	482.0	0.9553	1.044	$191.7^{+14.7}_{-13.1}$	33.1 ± 0.1	$3.06^{+0.23}_{-0.21}$	$78.9^{+10.3}_{-8.6}$	22.2 ± 0.1	$3.27^{+0.43}_{-0.36}$	$3.10^{+0.21}_{-0.18} \pm 0.13$
4.1784	3189.0	1.0398	1.054	$829.5^{+29.6}_{-28.0}$	30.0 ± 0.1	$2.01^{+0.07}_{-0.07}$	$282.8^{+18.3}_{-16.7}$	19.8 ± 0.1	$1.81^{+0.12}_{-0.11}$	$2.01^{+0.06}_{-0.06} \pm 0.08$
4.1888	524.6	1.0034	1.056	$145.0^{+13.0}_{-11.3}$	30.8 ± 0.1	$2.15^{+0.19}_{-0.17}$	$58.2^{+9.3}_{-7.5}$	20.3 ± 0.1	$2.28^{+0.36}_{-0.29}$	$2.18^{+0.17}_{-0.15} \pm 0.11$
4.1989	526.0	1.0156	1.057	$133.9^{+12.6}_{-10.9}$	30.7 ± 0.1	$1.96^{+0.18}_{-0.16}$	$62.8^{+8.8}_{-7.2}$	20.4 ± 0.1	$2.41^{+0.34}_{-0.28}$	$2.04^{+0.16}_{-0.14} \pm 0.09$
4.2092	518.0	1.0240	1.057	$136.2^{+12.4}_{-10.8}$	30.8 ± 0.1	$2.00^{+0.18}_{-0.16}$	$47.3^{+8.0}_{-6.4}$	20.1 ± 0.1	$1.86^{+0.31}_{-0.25}$	$1.97^{+0.16}_{-0.13} \pm 0.09$
4.2187	514.6	1.1701	1.056	$107.2^{+11.5}_{-9.9}$	28.1 ± 0.1	$1.52^{+0.16}_{-0.14}$	$38.4^{+7.4}_{-5.7}$	18.8 ± 0.1	$1.42^{+0.27}_{-0.21}$	$1.49^{+0.14}_{-0.12} \pm 0.08$
4.2263	1056.4	1.0228	1.056	$255.1^{+16.7}_{-15.1}$	30.7 ± 0.1	$1.85^{+0.12}_{-0.11}$	$96.9^{+11.1}_{-9.5}$	20.0 ± 0.1	$1.88^{+0.22}_{-0.18}$	$1.85^{+0.11}_{-0.09} \pm 0.08$
4.2357	530.3	1.0569	1.055	$121.2^{+12.0}_{-10.4}$	29.9 ± 0.1	$1.74^{+0.17}_{-0.15}$	$47.3^{+7.9}_{-6.3}$	19.8 ± 0.1	$1.78^{+0.30}_{-0.24}$	$1.75^{+0.15}_{-0.13} \pm 0.08$
4.2438	538.1	1.0464	1.056	$120.2^{+11.7}_{-10.1}$	29.5 ± 0.1	$1.74^{+0.17}_{-0.15}$	$46.7^{+8.0}_{-6.4}$	19.3 ± 0.1	$1.80^{+0.31}_{-0.25}$	$1.75^{+0.15}_{-0.13} \pm 0.09$
4.2580	828.4	1.0536	1.053	$189.0^{+14.6}_{-13.0}$	30.7 ± 0.1	$1.70^{+0.13}_{-0.12}$	$61.1^{+9.0}_{-7.4}$	20.0 ± 0.1	$1.47^{+0.22}_{-0.18}$	$1.64^{+0.11}_{-0.10} \pm 0.07$
4.2668	531.1	1.0238	1.053	$132.4^{+12.3}_{-10.7}$	29.9 ± 0.1	$1.96^{+0.18}_{-0.16}$	$42.1^{+7.7}_{-6.1}$	19.7 ± 0.1	$1.65^{+0.30}_{-0.24}$	$1.88^{+0.16}_{-0.13} \pm 0.08$
4.2777	175.7	1.0463	1.053	$39.1^{+7.2}_{-5.6}$	30.1 ± 0.1	$1.71^{+0.31}_{-0.24}$	$15.0^{+4.9}_{-3.3}$	19.6 ± 0.1	$1.75^{+0.57}_{-0.38}$	$1.71^{+0.28}_{-0.21} \pm 0.10$
4.3583	543.9	1.1749	1.051	$80.7^{+9.8}_{-8.2}$	26.4 ± 0.1	$1.15^{+0.14}_{-0.12}$	$26.7^{+6.2}_{-4.6}$	17.3 ± 0.1	$1.02^{+0.24}_{-0.18}$	$1.12^{+0.12}_{-0.10} \pm 0.05$
4.4156	1043.9	1.0714	1.052	$176.1^{+14.3}_{-12.6}$	29.7 ± 0.1	$1.28^{+0.10}_{-0.09}$	$57.7^{+9.1}_{-7.4}$	18.6 ± 0.1	$1.16^{+0.18}_{-0.15}$	$1.25^{+0.09}_{-0.08} \pm 0.05$
4.5995	586.9	1.1439	1.055	$80.1^{+9.8}_{-8.2}$	26.7 ± 0.1	$1.07^{+0.13}_{-0.11}$	$15.5^{+5.0}_{-3.4}$	16.2 ± 0.1	$0.60^{+0.19}_{-0.13}$	$0.92^{+0.11}_{-0.08} \pm 0.04$

plane perpendicular to the beam direction. For particle identification (PID), the TOF information and the specific energy deposit dE/dx in the MDC are combined to calculate a probability $P(h)$ for the particle hypotheses $h = \pi, K, p$. This probability corresponds to the p-value of observing the sum of squared residuals χ^2_{PID} between measured values and the expected values for the given particle species. The particle type with the largest probability is assigned to each track. In addition, we require a minimum probability of $P(h) > 10^{-5}$ to suppress background from those tracks for which none of the possible assignments has a high probability.

For photons, a minimum energy deposit in the calorimeter of 25 MeV in the barrel region ($|\cos\theta| < 0.80$) or of 50 MeV in the end-cap regions ($0.86 < |\cos\theta| < 0.92$) is required. In addition, the time information from the shower in the calorimeter relative to the event start time has to be less than 700 ns. Showers within 10° of the impact point of any charged track are discarded.

Only events containing exactly one good proton and one good antiproton candidate (and exactly one good π^+ and one good π^- candidate in the case of the $p\bar{p}\pi^+\pi^-\gamma\gamma$ final state) and at least two good photon candidates are retained. A four- (five-)constraint kinematic fit is performed to the $p\bar{p}\gamma\gamma$ ($p\bar{p}\pi^+\pi^-\pi^0$ with $\pi^0 \to \gamma\gamma$) hypothesis requiring four-momentum conservation between initial and final states and, if relevant, an additional mass constraint for the $\pi^0 \to \gamma\gamma$ decay. If more than one $\gamma\gamma$ combination in an event satisfies the above requirements, only the combination with the lowest kinematic fit χ^2 is kept for further analysis. Multiple combinations satisfying all requirements happens in about 12% (10%) in the case of the $p\bar{p}\gamma\gamma$ and $p\bar{p}\pi^+\pi^-\gamma\gamma$ final states, respectively. The resulting invariant mass spectra for the decays $\eta \to \gamma\gamma$, $\eta \to \pi^+\pi^-\pi^0$, and $\omega \to \pi^+\pi^-\pi^0$ are displayed for the data at $\sqrt{s} = 4.1784$ GeV in Fig. 1. According to the inclusive MC sample, backgrounds containing tracks misidentified as (anti)proton candidates are very rare and can be neglected. In the case of the $p\bar{p}\gamma\gamma$ final state, the main background channels are the processes $e^+e^- \to p\bar{p}$, $p\bar{p}\pi^0$, $p\bar{p}\omega$ with a subsequent $\omega \to \pi^0\gamma$ decay and $e^+e^- \to \gamma_{\mathrm{ISR}}J/\psi$ with a subsequent $J/\psi \to p\bar{p}$ decay. For the $p\bar{p}\pi^+\pi^-\gamma\gamma$ final state, the main background channels are $e^+e^- \to \Delta\bar{\Delta}\pi$, $e^+e^- \to p\bar{\Delta}\rho$, $e^+e^- \to p\bar{\Delta}\pi\pi$ and $e^+e^- \to p\bar{p}\rho\pi$ (the various possible charges of the Δ, $\bar{\Delta}$, ρ and π and overall charge conjugation are taken into account), which can all lead to the signal final state. No peaking backgrounds in the invariant mass distributions $m(\gamma\gamma)$ and $m(\pi^+\pi^-\pi^0)$ are found.

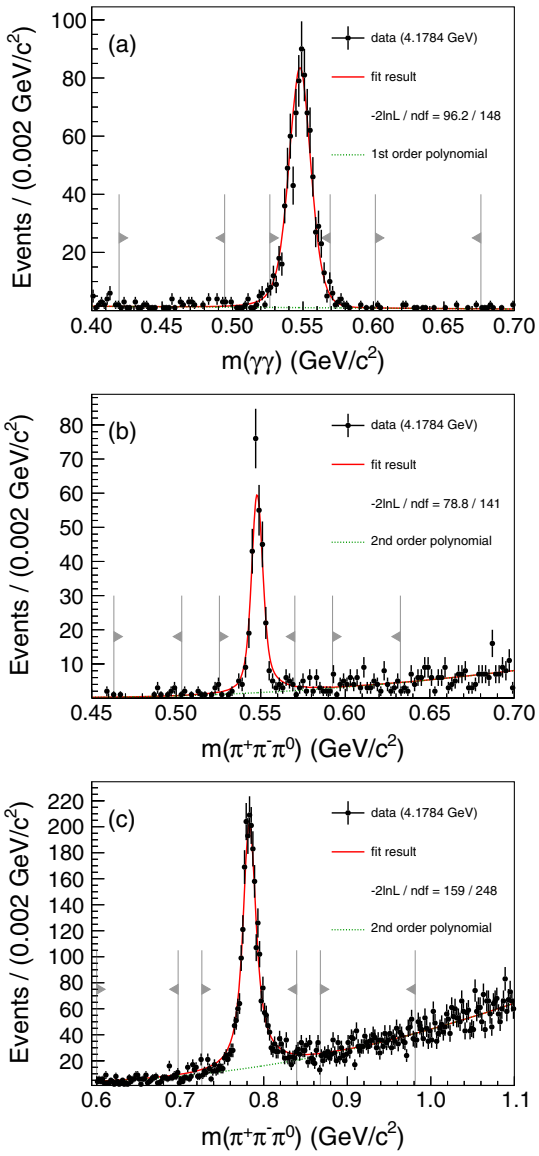

FIG. 1. Fits to the invariant mass of the (a) $\eta \to \gamma\gamma$, (b) $\eta \to \pi^+\pi^-\pi^0$, and (c) $\omega \to \pi^+\pi^-\pi^0$ systems. Black points represent data at the center-of-mass energy of $\sqrt{s} = 4.1784$ GeV, full (red) lines represent the total fit result and short-dashed (green) lines show the background contribution. The gray markers indicate signal and sideband regions.

The selection criteria with respect to the kinematic fit are optimized according to $\frac{s}{\sqrt{s+b}}$, where s and b are the number of signal and background events in the inclusive MC sample, that has been scaled to data, after requiring $\chi^2 < \chi^2_{\rm sel}$. In the case of the $p\bar{p}\gamma\gamma$ final state, $\chi^2 < 30$ is found as an optimal selection condition, whereas for the other two reactions the background is dominated by other processes leading to the $p\bar{p}\pi^+\pi^-\pi^0$ system so that no requirement is made on the χ^2 of the kinematic fit. This procedure is repeated with s' and b' being signal and background contributions determined directly from data using the η (ω) signal- and sidebands. The resulting selection condition agrees with the one determined from the inclusive MC sample within statistical uncertainties. As both the data and the inclusive MC samples at the other center-of-mass energies are significantly smaller than those at $\sqrt{s} = 4.1784$ GeV, we do not repeat this optimization, and the requirement $\chi^2 < 30$ for the $p\bar{p}\gamma\gamma$ final state is applied for all center-of-mass energies.

The number of signal events is determined from a fit to the invariant mass spectra (see Fig. 1). In the fit, the signal is described by a shape determined from reconstructed signal MC simulations convolved with a Gaussian function in order to account for a possible underestimation of the mass resolution in MC simulation. The η and ω mesons are described by relativistic Breit-Wigner distributions in the MC generator. The background is described by first- and second-order polynomial functions in the case of $\eta \to \gamma\gamma$ and $\eta(\omega) \to \pi^+\pi^-\pi^0$, respectively. In the first step, we perform a global binned maximum likelihood fit to the sum of the data at all center-of-mass energies, determining a width of the Gaussian smearing functions as well as a background shape for each of the three processes under study. A binned maximum likelihood fit is then performed to each dataset and process individually, with only the signal and background yields as free parameters. The signal and background shape are fixed to the result of the global fit in order to obtain reliable results from all sample sizes. We repeat this procedure using different smaller subsets of the data at different $\sqrt{s}$ and find no significant difference. Thus, it is reasonable to assume that the background shape does not change with s. The number of signal events in process i for each $\sqrt{s}$ is then found by applying $N^i_{\rm sig}(s) = n_{\rm sr} - n_{\rm bg,sr}$. Here, $n_{\rm sr}$ is the number of events in the signal region (defined as a symmetric region around the nominal η (ω) mass containing 95% of the events according to the signal shape), and $n_{\rm bg,sr}$ is the number of background events in the same region derived from the polynomial function (see Fig. 1).

IV. EFFICIENCY DETERMINATION

We define the efficiency, $\epsilon^i(s)$, according to

$$\epsilon^i(s) = \frac{N^i_{\rm acc}(s)}{N^i_{\rm gen}(s)}, \tag{1}$$

where $N^i_{\rm acc}(s)$ is the number of reconstructed signal events and $N^i_{\rm gen}(s)$ is the total size of the signal MC sample for the process i at a center-of-mass energy $\sqrt{s}$. If the efficiency is not constant over the full n-particle phase-space, Eq. (1) only holds if the signal MC sample properly reflects data in all relevant coordinates $\vec{x} = \{p_p, \theta_p, \phi_p, p_{\bar{p}}, \theta_{\bar{p}}, \phi_{\bar{p}}, \ldots\}$. Since the data distribution is *a priori* unknown, we will perform a partial wave analysis of the data in order to reweight our MC sample.

The isobar model [29] is used in the partial wave analysis by decomposing the full $e^+e^- \to \gamma^* \to p\bar{p}\eta$ and $e^+e^- \to \gamma^* \to p\bar{p}\omega$ processes into a sequence of two-body decays. Each two-body decay is described in the helicity formalism [30], with a two-body decay amplitude for the decay $a \to bc$ given as

$$A^{J_a,\lambda_a}_{\lambda_b,\lambda_c}(a \to bc) = \sqrt{\frac{2J_a+1}{4\pi}} D^{J_a *}_{\lambda_a,\lambda}(\phi,\theta,0) F^{J_a}_{\lambda_b,\lambda_c}, \quad (2)$$

where J_a and λ_a are the spin and the helicity of mother particle a, λ_b, and λ_c are the helicities of the two daughter particles b and c, $\lambda = \lambda_b - \lambda_c$, $D^J_{\lambda_a,\lambda}$ is Wigner's D-function, and ϕ and θ are the azimuthal and polar helicity angles of b in the rest-frame of a. We expand the helicity amplitudes $F^{J_a}_{\lambda_b,\lambda_c}$ into states with a defined set of J^{PC}, L and S quantum numbers using the transformation

$$F^{J_a}_{\lambda_b,\lambda_c} = \sum_{L,S} \sqrt{\frac{2L+1}{2J_a+1}} \cdot \langle L,0;S,\lambda|J_a,\lambda\rangle \cdot \langle J_b,\lambda_b;J_c,-\lambda_c|S,\lambda\rangle, \quad (3)$$

where $\langle\ldots\rangle$. denote Clebsch-Gordan coefficients and S and L are limited by $\vec{S} = \vec{J}_b + \vec{J}_c$ and $\vec{J}_a = \vec{L} + \vec{S}$ as well as conservation of parity and C-parity. The η meson is treated as a stable particle in the amplitude analysis, whereas the three-body decay of the ω meson is described by a three-body amplitude according to Ref. [31]. Blatt-Weisskopf barrier factors [30] are used for both the production $\gamma^* \to ad$ and the two-body decay $a \to bc$ according to Ref. [31]. The dynamical part of the amplitude is described by relativistic Breit-Wigner amplitudes of the form

$$BW(m) = \frac{m_0 \Gamma B_L(q,q_0)}{m_0^2 - m^2 - i\frac{\rho(m)}{\rho(m_0)} m_0 \Gamma B_L^2(q,q_0)}$$

with

$$\rho(m) = \sqrt{\left(1 - \left(\frac{m_b+m_c}{m}\right)^2\right) \cdot \left(1 - \left(\frac{m_b-m_c}{m}\right)^2\right)}. \quad (4)$$

Here, m_0 and Γ are mass and width of the resonance a decaying to daughter-particles b and c. $B_L(q,q_0) = \frac{b_L(q)}{b_L(q_0)}$ is the ratio of the Blatt-Weisskopf barrier factors $b_L(q)$ at the linear momentum q of particle b in the rest-frame of a (q_0 is the momentum at $m = m_0$) and $\rho(m)$ is the phase-space factor. Only the line shape of the η and ω mesons is not described in this way. Here we employ the signal MC simulations that are used for normalization in the partial wave analysis for the line-shapes. For the $e^+e^- \to p\bar{p}\eta$ process, we include the J/ψ resonance (using a Voigt distribution) and other possible $J^{PC} = 1^{--}$ and $J^{PC} = 3^{--}$ contributions in the $p\bar{p}$ system. We also include one $J^P = \frac{1}{2}^{-(+)}$ and one $J^P = \frac{3}{2}^{+(-)}$ resonance contribution for the $\eta p(\bar{p})$ system. For the $e^+e^- \to p\bar{p}\omega$ process, only intermediate states that decay to the $p\bar{p}$ system are included. For each of the three possible quantum numbers $J^{PC} = 0^{-+}, 0^{++}, 2^{++}$ we include a phase-space contribution that is constant as a function of $m(p\bar{p})$ as well as two resonant contributions. All masses and widths of intermediate states are free parameters in the fit, apart from the J/ψ contribution, where mass and width are fixed to the values given in the PDG [25]. Note that the aim of this partial wave analysis is only to describe the data accurately enough to enable an accurate determination of the efficiency.

The partial wave analysis is performed as an unbinned maximum likelihood fit using the software package PAWIAN [32]. Details on likelihood construction in PAWIAN can be found in Refs. [31–33]. The remaining background events underneath the η (ω) peaks are accounted for in the partial wave analysis by adding the sidebands defined in Fig. 1 to the likelihood with negative weights in such a way that the combined sideband weight is equal to the integral of the background function in the signal region.

The data for the two decays $\eta \to \gamma\gamma$ and $\eta \to \pi^+\pi^-\pi^0$ are fitted simultaneously with all amplitudes fully constrained between the two processes apart from an overall scaling factor. The results of the partial wave analysis for the different processes are displayed in Fig. 2 for the high statistics data at a center-of-mass energy of $\sqrt{s} = 4.1784$ GeV. In general, the fits have a similar quality for all center-of-mass energies. As the efficiency only varies slowly over the Dalitz plot, the remaining small differences between the data and the fit solution are not important in the determination of the average efficiency. For each energy point, we obtain event weights, $w(\vec{x})$, from the partial wave analysis as a function of the coordinates in the n-particle phase-space. The event weights correspond to the absolute squared of the full amplitude, normalized such that $\sum_{j=0}^{N^i_{\rm acc}(s)} w(\vec{x}_j)$ corresponds to the number of observed signal events. These event weights are used to determine the efficiency $\epsilon^i(s)$ as

$$\epsilon^i(s) = \frac{\sum_{j=0}^{N^i_{\rm acc}(s)} w(\vec{x}_j)}{\sum_{j=0}^{N^i_{\rm gen}(s)} w(\vec{x}_j)}. \quad (5)$$

The efficiencies obtained in this way are summarized in Tables I and II.

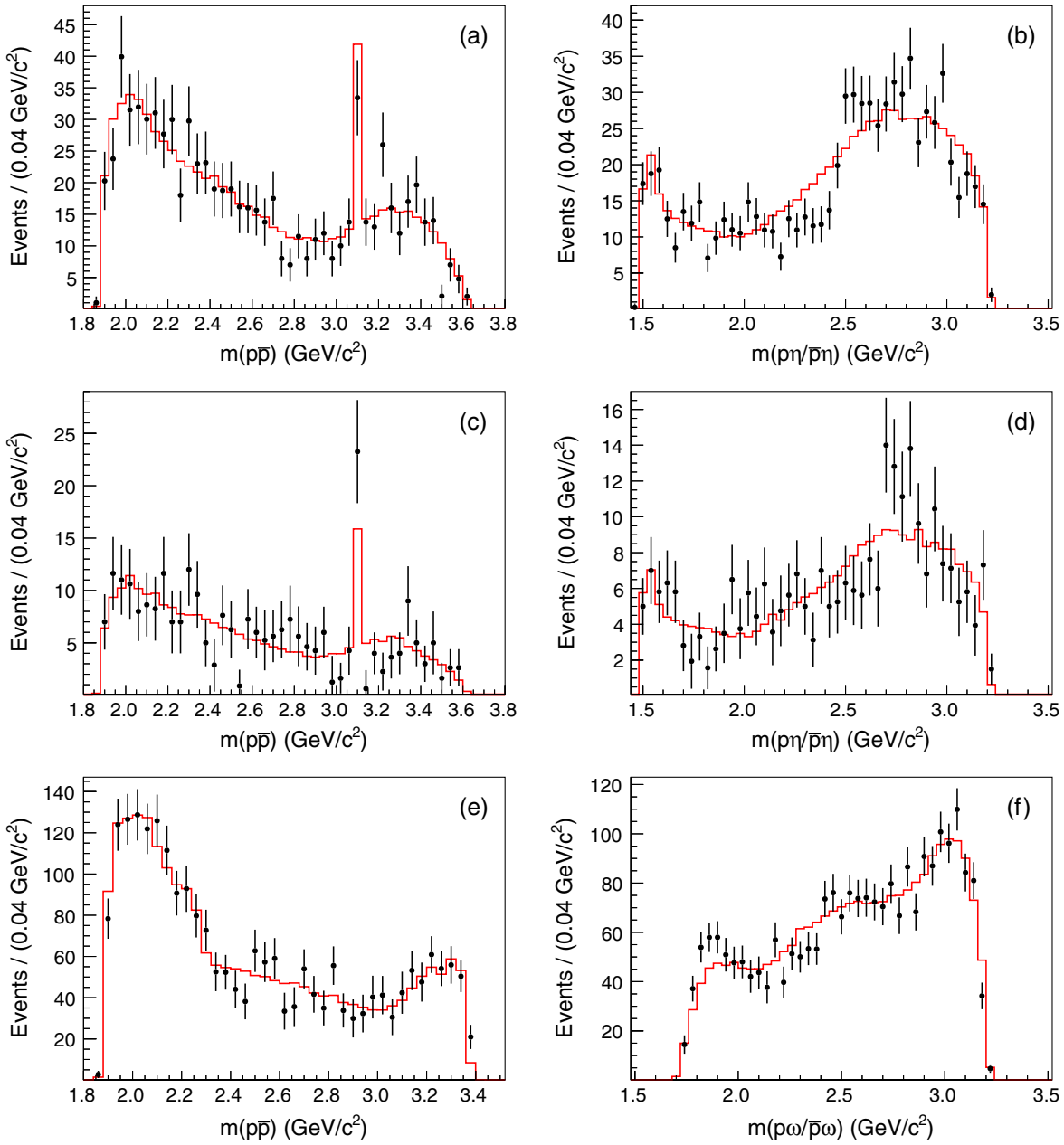

FIG. 2. Results of the partial wave analysis of the $e^+e^- \to p\bar{p}\eta$ process with subsequent $\eta \to \gamma\gamma$ (a, b) and $\eta \to \pi^+\pi^-\pi^0$ decays (c, d) and the $e^+e^- \to p\bar{p}\omega$ process (e, f) for the data at a center-of-mass energy of $\sqrt{s} = 4.1784$ GeV. The left column shows the invariant mass of the $p\bar{p}$ system, the right column the invariant mass of the $p\eta$ ($p\omega$) system. Black points correspond to data, full (red) lines show the result of the amplitude analysis.

V. DETERMINATION OF BORN CROSS SECTIONS

The Born cross section of each signal process is determined by

$$\sigma_B(s) = \frac{N(s)}{L(s) \cdot (1+\delta_r(s)) \cdot \frac{1}{|1-\Pi|^2} \cdot \epsilon(s) \cdot B}, \qquad (6)$$

where $N(s)$ is the number of signal events observed in the data sample at center-of-mass energy $\sqrt{s}$, $L(s)$ is the corresponding integrated luminosity determined using Bhabha scattering [34], $\delta_r(s)$ and $\frac{1}{|1-\Pi|^2}$ are corrections accounting for initial state radiation and vacuum polarization, $\epsilon(s)$ is the efficiency and B is the product of branching ratios involved in the decay. The correction $\frac{1}{|1-\Pi|^2}$ is calculated with the alphaQED software package [35] with an accuracy of 0.5%. Initial state radiation depends on the shape of the cross section and can, in general, have an effect on the efficiency. This is treated in an iterative procedure starting from a flat energy dependence of the Born cross section $\sigma_B(s)$. We consider two successive

TABLE II. Summary of the Born cross sections σ_B of the process $e^+e^- \to p\bar{p}\omega$ for the datasets at different center-of-mass energies $\sqrt{s}$, integrated luminosity L, radiative corrections $1+\delta_r$, vacuum polarization correction $\frac{1}{|1-\Pi|^2}$, number of observed events N, and the efficiency ϵ.

$\sqrt{s}$ (GeV)	L (pb^{-1})	$(1+\delta_r)$	$\frac{1}{\lvert 1-\Pi\rvert^2}$	N	ε (%)	σ_B (pb)
3.7730	2931.8	0.8978	1.057	$4623.7^{+79.2}_{-77.4}$	30.9 ± 0.1	$6.11^{+0.10}_{-0.10} \pm 0.41$
3.8695	224.0	0.9417	1.051	$285.7^{+19.9}_{-18.2}$	30.7 ± 0.1	$4.76^{+0.33}_{-0.30} \pm 0.32$
4.0076	482.0	0.9832	1.044	$485.4^{+25.0}_{-23.3}$	30.8 ± 0.1	$3.71^{+0.19}_{-0.17} \pm 0.26$
4.1784	3189.0	1.0220	1.054	$2357.9^{+53.9}_{-52.2}$	29.0 ± 0.1	$2.68^{+0.06}_{-0.06} \pm 0.18$
4.1888	524.6	1.0406	1.056	$370.4^{+22.4}_{-20.7}$	28.2 ± 0.1	$2.58^{+0.16}_{-0.14} \pm 0.18$
4.1989	526.0	1.0217	1.057	$380.3^{+22.1}_{-20.5}$	27.6 ± 0.1	$2.76^{+0.16}_{-0.15} \pm 0.19$
4.2092	518.0	1.0393	1.057	$355.7^{+21.3}_{-19.6}$	28.3 ± 0.1	$2.51^{+0.15}_{-0.14} \pm 0.17$
4.2187	514.6	1.0869	1.056	$319.3^{+20.4}_{-18.7}$	27.0 ± 0.1	$2.27^{+0.14}_{-0.13} \pm 0.16$
4.2263	1056.4	1.0145	1.056	$733.8^{+30.9}_{-29.2}$	28.6 ± 0.1	$2.57^{+0.11}_{-0.10} \pm 0.18$
4.2357	530.3	1.0189	1.055	$371.0^{+22.0}_{-20.3}$	28.6 ± 0.1	$2.57^{+0.15}_{-0.14} \pm 0.18$
4.2438	538.1	1.0463	1.056	$353.4^{+21.5}_{-19.8}$	28.7 ± 0.1	$2.36^{+0.14}_{-0.13} \pm 0.17$
4.2580	828.4	1.0424	1.053	$539.1^{+26.4}_{-24.7}$	28.8 ± 0.1	$2.34^{+0.11}_{-0.11} \pm 0.16$
4.2668	531.1	1.0287	1.053	$347.0^{+21.3}_{-19.6}$	26.3 ± 0.1	$2.60^{+0.16}_{-0.15} \pm 0.18$
4.2777	175.7	1.0823	1.053	$106.4^{+12.8}_{-11.0}$	25.4 ± 0.1	$2.37^{+0.29}_{-0.25} \pm 0.17$
4.3583	543.9	1.0569	1.051	$300.3^{+19.7}_{-18.0}$	26.2 ± 0.1	$2.15^{+0.14}_{-0.13} \pm 0.15$
4.4156	1043.9	1.0554	1.052	$540.0^{+26.0}_{-24.4}$	26.9 ± 0.1	$1.96^{+0.09}_{-0.09} \pm 0.14$
4.5995	586.9	1.1230	1.055	$210.4^{+16.5}_{-14.8}$	25.1 ± 0.1	$1.37^{+0.11}_{-0.10} \pm 0.10$

iterations converged if $\kappa_i/\kappa_{i-1} = 1$ within statistical uncertainties, where $\kappa(s) = \epsilon(s) \cdot (1+\delta_r(s))$ is the product of the efficiency and a radiative correction factor $1+\delta_r(s)$ obtained from the ConExc MC generator. The product of branching fractions is given by $B = \mathrm{Br}(\eta \to \gamma\gamma)$ for the $e^+e^- \to p\bar{p}\eta(\to \gamma\gamma)$ process, $B = \mathrm{Br}(\eta \to \pi^+\pi^-\pi^0) \cdot \mathrm{Br}(\pi^0 \to \gamma\gamma)$ for the $e^+e^- \to p\bar{p}\eta(\to \pi^+\pi^-\pi^0)$ process and $B = \mathrm{Br}(\omega \to \pi^+\pi^-\pi^0) \cdot \mathrm{Br}(\pi^0 \to \gamma\gamma)$ for the $e^+e^- \to p\bar{p}\omega(\to \pi^+\pi^-\pi^0)$ process. A combined Born cross section σ_B is determined for the two different η decay modes by using a weighted least squares method [36]. The resulting cross sections are displayed in Fig. 3 and all necessary values for their calculation are summarized in Tables I and II.

VI. SYSTEMATIC UNCERTAINTIES

Various sources of systematic uncertainties contributing to the measurement of the $e^+e^- \to p\bar{p}\eta$ and $e^+e^- \to p\bar{p}\omega$ Born cross sections have been considered.

The uncertainty of the integrated luminosity determined using Bhabha scattering is 1% [34]. The systematic uncertainty of the tracking efficiency has been determined using a $J/\psi \to p\bar{p}\pi^+\pi^-$ control sample in Ref. [37] as 1% per track. Similarly, systematic uncertainties of photon detection efficiencies have been studied using a $J/\psi \to \rho\pi$ control sample [38] and were found to be 1% per photon. For PID efficiency, a systematic uncertainty of 1% per proton and 1% per pion are taken from Ref. [12,39]. For multiple particles, each of the track-finding, PID, and photon efficiency uncertainties are added linearly [12,37–39]. Uncertainties on the branching fractions are taken from the PDG [25]. With regard to possible differences between data and MC concerning the kinematic fit, where a selection condition of $\chi^2 < 30$ is applied in the case of the $e^+e^- \to p\bar{p}\eta(\to \gamma\gamma)$ mode, this selection condition is varied between $\chi^2 < 5$ and $\chi^2 < 55$ in steps of $\delta\chi^2 = 5$. The resulting Born cross section is determined and compared with the nominal value $R = \frac{\sigma_{\mathrm{step}}}{\sigma_{\mathrm{nom}}}$. We take the standard deviation of a weighted sample of the ratio R as the systematic uncertainty due to potential differences in the χ^2 distributions between data and MC simulation. Here, $1/\delta R$ is used as the weight, where δR is the uncertainty taking into account the sizable correlation between the event samples. The nominal symmetric signal region containing 95% of the total signal is altered to a set of both smaller and larger signal regions and we determine the resulting Born cross sections. As outlined above, we take the standard deviation of a sample of ratios R weighted by the inverse of the statistical uncertainty as the systematic uncertainty resulting from possible deviations in the tails of the signal distribution between data and MC simulation. For the background description, the polynomial shapes

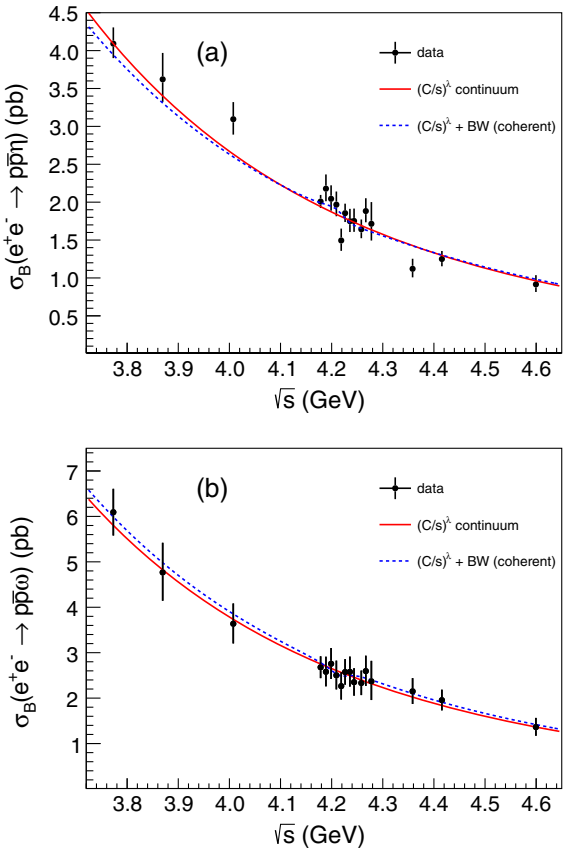

FIG. 3. Born cross sections of the $e^+e^- \to p\bar{p}\eta$ (a) and $e^+e^- \to p\bar{p}\omega$ (b) processes as a function of the center-of-mass energy. Black points represent our result including both statistical and systematic uncertainties. The full (red) and long-dashed (blue) lines represent the fits using a continuum contribution and a Breit-Wigner coherently added to the continuum contribution, respectively. The fits displayed ($m = 4.2187$ GeV/c^2 and $\Gamma = 44$ MeV) are those for the current world average parameters of the $\psi(4230)$ [25].

were increased by one order from the nominal first order polynomial used for the $\eta \to \gamma\gamma$ invariant mass spectrum, and the second order polynomial in the case of the $\eta \to \pi^+\pi^-\pi^0$ and $\omega \to \pi^+\pi^-\pi^0$ invariant mass spectra. The fits are then repeated and the difference to the nominal results is taken as a systematic uncertainty. For the radiative correction factor, we performed five additional iterations and found no difference beyond the statistical uncertainty. This contribution to the systematic uncertainty is therefore neglected. In addition, the radiative correction factor depends on how the cross section is modeled in the MC simulation. In our nominal approach, we use our discrete set of measurements as an input and cross sections at intermediate values of the c.m. energy are interpolated using splines. In an alternative approach, we use our fit to the Born cross sections as an input in the simulations instead. We take the average difference between the two outcomes of 2.5% and 0.7% for the $p\bar{p}\eta$ and $p\bar{p}\omega$ reactions, respectively, as systematic uncertainties with respect to the choice of cross section model. Concerning the efficiency as a result of the amplitude analysis, we determine sets of efficiencies by replacing the fit solution at a given c.m. energy with the solution at neighboring energies (wherever these are reasonably close) as well as with a solution that is obtained when the data sets at 4.1888, 4.1989, 4.2092, 4.2187, and 4.2263 GeV are combined in a single fit. The average difference of the efficiencies of 1.0% and 2.5% for the $p\bar{p}\eta$ and $p\bar{p}\omega$ reactions are taken as the systematic uncertainties on the efficiency due to the uncertainty in the PWA parameters.

TABLE III. Summary of systematic uncertainties in percent for the data at $\sqrt{s} = 4.1784$ GeV.

	$\eta \to \gamma\gamma$	$\eta \to \pi^+\pi^-\pi^0$	$\omega \to \pi^+\pi^-\pi^0$
Luminosity	1.0	1.0	1.0
Tracking efficiency	2.0	4.0	4.0
Photon detection	2.0	2.0	2.0
Particle identification	2.0	4.0	4.0
Branching fraction	0.5	1.2	0.8
Cross section model	2.5	2.5	0.7
PWA efficiency	1.0	1.0	2.5
χ^2 cut	1.9		
Signal region	0.6	0.8	0.8
Background description	0.7	1.5	0.3
Total	5.0	7.0	6.7

The systematic uncertainties are summarized in Table III for the data at a center-of-mass energy of $\sqrt{s} = 4.1784$ GeV. The total systematic uncertainty is obtained by adding each contribution in quadrature. Correlated systematic uncertainties in the two $e^+e^- \to p\bar{p}\eta$ processes are accounted for in the calculation of the combined Born cross section following Ref. [36].

VII. SEARCH FOR RESONANT CONTRIBUTIONS

The final Born cross sections for the $e^+e^- \to p\bar{p}\eta$ and $e^+e^- \to p\bar{p}\omega$ processes are displayed in Fig. 3. In order to search for possible $e^+e^- \to V \to p\bar{p}\eta$ ($e^+e^- \to V \to p\bar{p}\omega$) resonant contributions, we perform two different fits. In the first fit, only a nonresonant contribution of the type

$$\sigma_{\rm nr}(s) = \left(\frac{C}{\sqrt{s}}\right)^{\lambda} \tag{7}$$

defined in Ref. [12] is used. Here, C and λ are free parameters in the fit. The second fit includes a single Breit-Wigner amplitude of the form

$$A_{\rm res}(s) = A_V\left(\frac{m\Gamma}{s^2 - m^2 + im\Gamma}\right) \tag{8}$$

that is coherently added to the nonresonant term.

Unbinned maximum likelihood fits are performed where the likelihood $L(x;\Theta)$ given the data x and the fit parameters $\Theta = (C, \lambda, \mathrm{Re}(A_V), \mathrm{Im}(A_V), m, \Gamma)$ is defined as the product $L(x;\Theta) = \prod_{i,j} L_{ij}(\Theta)$, where L_{ij} is a set of likelihood functions, one each for each dataset i and decay mode j. These likelihood functions are transformed such that they only depend on the expected number of signal events $N \equiv N_{ij}(\Theta)$ which can be calculated for each dataset according to Eq. (6). The likelihood $L_{ij}(N)$ is then obtained from data via a likelihood scan of the number of signal events in the invariant mass distributions of the meson decay systems. These likelihood scans are parametrized by asymmetric Gaussian distributions. Incorporating the systematic uncertainties of dataset i and process j, the likelihood is

$$L_{ij}(N) = \frac{1}{\sqrt{2\pi\left(\left(\frac{\sigma_{L,ij}+\sigma_{R,ij}}{2}\right)^2 + \sigma^2_{\mathrm{sys},ij}\right)}} \cdot e^{-\frac{(N_{ij}-\mu_{ij})^2}{2(\sigma_k^2+\sigma^2_{\mathrm{sys},ij})}}$$
$$\text{with} \quad \sigma_k = \begin{cases} \sigma_{L,ij}, N_{ij} \le \mu_{ij} \\ \sigma_{R,ij}, N_{ij} > \mu_{ij} \end{cases}. \tag{9}$$

In the fit, all systematic uncertainties apart from the one on the branching ratio of the meson decays are considered uncorrelated between the different c.m. energies. While there will be some unknown correlation of the remaining systematic uncertainty between two c.m. energies, our assumption of a vanishing correlation leads to the most conservative upper limit estimation. We find no evidence for a resonant contribution from the fits and set upper limits at the 90% confidence level. As the resonant contribution is added coherently, the fit finds two ambiguous solutions for constructive and destructive interference by construction. The upper limits are obtained by integrating $L(x;\Theta) = \prod_{i,j} L_{ij}(\Theta)$ according to

$$\frac{\int_{-\infty}^{\sigma_V^{\mathrm{UL}}} L(x,\Theta)\pi(\Theta)d\sigma_V}{\int_{-\infty}^{\infty} L(x,\Theta)\pi(\Theta)d\sigma_V} = 0.90, \tag{10}$$

where the prior $\pi(\Theta)$ is given by

$$\pi(\Theta) = \begin{cases} 1, & \sigma_V \ge 0 \\ 0, & \sigma_V < 0 \end{cases}. \tag{11}$$

The procedure outlined above is repeated with a step size of 1 MeV for different masses m in the range 4 GeV/c^2 < m < 4.4 GeV/c^2 and widths Γ in the range 40 MeV < Γ < 300 MeV for a potential resonant contribution. The results are shown in Fig. 4.

The most stringent upper limits are found for resonant contributions with mass $m = 4.390$ GeV/c^2 ($m = 4.399$ GeV/c^2) and width $\Gamma = 40$ MeV ($\Gamma = 297$ MeV) in the $p\bar{p}\eta$ ($p\bar{p}\omega$) channel with values of 4.56 pb and 7.69 pb at the 90% CL, respectively. The upper limits for a resonant contribution of the $\psi(4230)$, using current world average values for mass ($m = 4.2187$ GeV/c^2) and width ($\Gamma = 44$ MeV) [25] are 7.5 pb and 10.4 pb at the 90% CL, respectively.

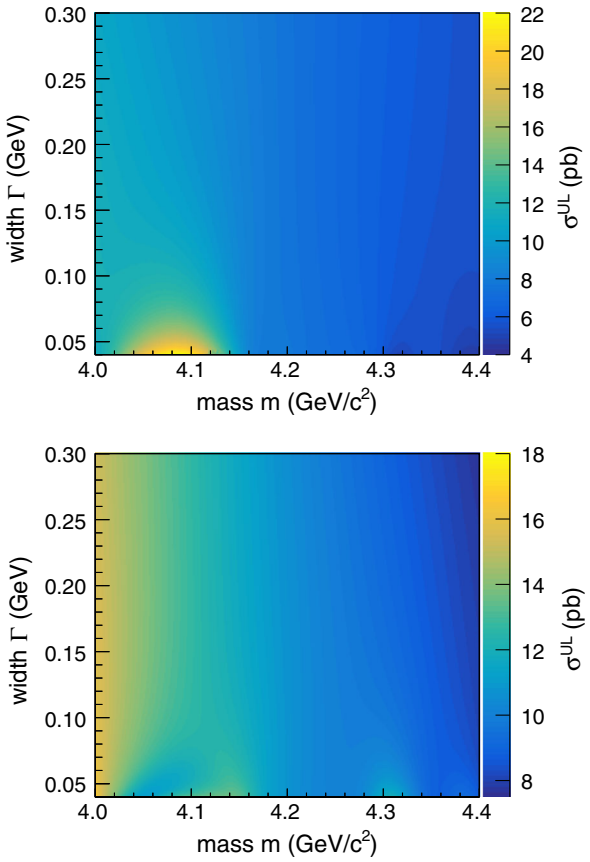

FIG. 4. Upper limits on a possible resonant contribution with mass m and width Γ for the two processes $e^+e^- \to p\bar{p}\eta$ (top) and $e^+e^- \to p\bar{p}\omega$ (bottom). All values displayed here are tabulated in the Supplemental Material [40].

VIII. SUMMARY

The processes $e^+e^- \to p\bar{p}\eta$ and $e^+e^- \to p\bar{p}\omega$ have been studied using 14.7 fb^{-1} of electron-positron annihilation data at 17 different center-of-mass energies between 3.7730 GeV and 4.5995 GeV. Both processes are clearly identified at all center-of-mass energies and Born cross sections are determined. We find no evidence for a resonant contribution from a fit to the $e^+e^- \to p\bar{p}\eta$ and $e^+e^- \to p\bar{p}\omega$ Born cross sections, and set upper limits at the 90% confidence level for a wide range of resonance parameters m and Γ. Using the approach outlined in Ref. [17], these upper limits will serve as valuable input for model calculations of the processes $p\bar{p} \to V\eta$ and $p\bar{p} \to V\omega$ for the upcoming PANDA experiment.

ACKNOWLEDGMENTS

The BESIII collaboration thanks the staff of BEPCII and the IHEP computing center for their strong support. This work is supported in part by National Key Basic Research Program of China under Contract No. 2015CB856700; National Natural Science Foundation of China (NSFC) under Contracts No. 11625523, No. 11635010, No. 11735014, No. 11822506, No. 11835012, No. 11935015, No. 11935016, No. 11935018, No. 11961141012; the Chinese Academy of Sciences (CAS) Large-Scale Scientific Facility Program; Joint Large-Scale Scientific Facility Funds of the NSFC and CAS under Contracts No. U1732263, No. U1832207; CAS Key Research Program of Frontier Sciences under Contracts No. QYZDJ-SSW-SLH003, No. QYZDJ-SSW-SLH040; 100 Talents Program of CAS; INPAC and Shanghai Key Laboratory for Particle Physics and Cosmology; ERC under Contract No. 758462; European Union Horizon 2020 research and innovation programme under Marie Sklodowska-Curie grant agreement No. 894790; German Research Foundation DFG under Contracts Nos. Collaborative Research Center CRC 1044, FOR 2359, 443159800, Research Training Group 2149; Istituto Nazionale di Fisica Nucleare, Italy; Ministry of Development of Turkey under Contract No. DPT2006K-120470; National Science and Technology fund; STFC (United Kingdom); The Knut and Alice Wallenberg Foundation (Sweden) under Contract No. 2016.0157; The Royal Society, UK under Contracts No. DH140054, No. DH160214; The Swedish Research Council; Olle Engkvist Foundation under Contract No. 200-0605; U.S. Department of Energy under Contracts No. DE-FG02-05ER41374, No. DE-SC-0012069.

[1] S. K. Choi *et al.* (Belle Collaboration), Phys. Rev. Lett. **91**, 262001 (2003).

[2] M. Ablikim *et al.* (BESIII Collaboration), Phys. Rev. Lett. **110**, 252001 (2013).

[3] B. Aubert *et al.* (*BABAR* Collaboration), Phys. Rev. Lett. **95**, 142001 (2005).

[4] M. Ablikim *et al.* (BESIII Collaboration), Phys. Rev. Lett. **118**, 092001 (2017).

[5] M. Ablikim *et al.* (BESIII Collaboration), Phys. Rev. Lett. **118**, 092002 (2017).

[6] M. Ablikim *et al.* (BESIII Collaboration), Phys. Rev. D **96**, 032004 (2017).

[7] M. Ablikim *et al.* (BESIII Collaboration), Phys. Rev. Lett. **122**, 102002 (2019).

[8] M. Ablikim *et al.* (BESIII Collaboration), Phys. Rev. Lett. **114**, 092003 (2015); Phys. Rev. D **99**, 091103 (2019).

[9] M. Ablikim *et al.* (BESIII Collaboration), Phys. Rev. D **86**, 071101 (2012).

[10] M. Ablikim *et al.* (BESIII Collaboration), Phys. Rev. D **91**, 112005 (2015).

[11] M. Ablikim *et al.* (BESIII Collaboration), Phys. Rev. D **102**, 031101 (2020).

[12] M. Ablikim *et al.* (BESIII Collaboration), Phys. Lett. B **771**, 45 (2017).

[13] M. Ablikim *et al.* (BESIII Collaboration), Phys. Lett. B **774**, 78 (2017).

[14] M. Ablikim *et al.* (BESIII Collaboration), Phys. Rev. D **98**, 032014 (2018).

[15] M. Ablikim *et al.* (BESIII Collaboration), Phys. Rev. D **99**, 072005 (2019).

[16] M. Ablikim *et al.* (BESIII Collaboration), Phys. Rev. D **99**, 012003 (2019).

[17] A. Lundborg, T. Barnes, and U. Wiedner, Phys. Rev. D **73**, 096003 (2006).

[18] M. F. M. Lutz *et al.* (PANDA Collaboration), arXiv:0903.3905.

[19] N. Brambilla, S. Eidelman, C. Hanhart, A. Nefediev, C.-P. Shen, C. E. Thomas, A. Vairo, and C.-Z. Yuan, Phys. Rep. **873**, 1 (2020).

[20] M. Ablikim *et al.* (BESIII Collaboration), Nucl. Instrum. Methods Phys. Res., Sect. A **614**, 345 (2010).

[21] C. H. Yu *et al.*, Joint Accelerator Conferences Website JACoW, in *Proceedings of IPAC2016*, Busan, Korea, 2016, https://doi.org/10.18429/JACoW-IPAC2016-TUYA01.

[22] X. Li *et al.*, Radiat. Detect. Technol. Methods **1**, 13 (2017); Y. X. Guo *et al.*, Radiat. Detect. Technol. Methods **1**, 15 (2017).

[23] S. Agostinelli *et al.* (GEANT4 Collaboration), Nucl. Instrum. Methods Phys. Res., Sect. A **506**, 250 (2003).

[24] R.-G. Ping *et al.*, Chin. Phys. C **40**, 113002 (2016).

[25] M. Tanabashi *et al.* (Particle Data Group), Phys. Rev. D **98**, 030001 (2018) and 2019 online update.

[26] D. J. Lange, Nucl. Instrum. Methods Phys. Res., Sect. A **462**, 152 (2001); R. G. Ping, Chin. Phys. C **32**, 599 (2008).

[27] J. C. Chen, G. S. Huang, X. R. Qi, D. H. Zhang, and Y. S. Zhu, Phys. Rev. D **62**, 034003 (2000); R. L. Yang, R. G. Ping, and H. Chen, Chin. Phys. Lett. **31**, 061301 (2014).

[28] E. Richter-Was, Phys. Lett. B **303**, 163 (1993).

[29] D. Herndon, P. Soding, and R. J. Cashmore, Phys. Rev. D **11**, 3165 (1975).

[30] S. U. Chung, Phys. Rev. D **57**, 431 (1998); **48**, 1225 (1993); **56**, 4419(E) (1997); S. U. Chung and J. M. Friedrich, Phys. Rev. D **78**, 074027 (2008).

[31] M. Ablikim *et al.* (BESIII Collaboration), Phys. Rev. D **100**, 052012 (2019).

[32] B. Kopf *et al.*, *Proceedings of 11th International Conference on Low Energy Antiproton Physics (LEAP2013)*, Hyperfine

Interact (Springer, 2014), Vol. 229, p. 69, https://doi.org/10.1007/s10751-014-1039-2.
[33] M. Albrecht *et al.* (Crystal Barrel Collaboration), Eur. Phys. J. C **80**, 453 (2020).
[34] M. Ablikim *et al.* (BESIII Collaboration), Chin. Phys. C **39**, 093001 (2015).
[35] F. Jegerlehner, Nuovo Cimento C **034S1**, 31 (2011).
[36] G. D'Agostini, Nucl. Instrum. Methods Phys. Res., Sect. A **346**, 306 (1994).
[37] W.-L. Yuan, X.-C. Ai, X.-B. Ji, S.-J. Chen, Y. Zhang, L.-H. Wu, L.-L. Wang, and Y. Yuan, Chin. Phys. C **40**, 026201 (2016).
[38] M. Ablikim *et al.* (BESIII Collaboration), Phys. Rev. D **81**, 052005 (2010).
[39] M. Ablikim *et al.* (BESIII Collaboration), Phys. Rev. D **86**, 092009 (2012).
[40] See Supplemental Material at http://link.aps.org/supplemental/10.1103/PhysRevD.104.092008 for tabulated values of the upper limits as a function of resonance mass and width.